Running head: Growth dynamics and osteoarthritis

Characterisation of growth plate dynamics in murine models of osteoarthritis

Hasmik J. Samvelyan[1,2], Kamel Madi[3], Anna E. Törnqvist[4,5], Behzad Javaheri[6], Katherine A. Staines[1,2]

[1] School of Pharmacy and Biomolecular Studies, University of Brighton, Brighton, UK

[2] Centre for Stress and Age-Related Disease, University of Brighton, Brighton, UK

[3] 3Dmagination Ltd, Harwell Campus, Didcot, UK

[4] Rheumatology and Bone Diseases Unit, Centre for Genomic and Experimental Medicine, MRC Institute of Genetics and Molecular Medicine, University of Edinburgh, Edinburgh, UK

[5] Centre for Bone and Arthritis Research, University of Gothenburg, Gothenburg, Sweden

[6] School of Mathematics, Computer Science and Engineering, City University of London, London, UK

Corresponding authors

Katherine Ann Staines, University of Brighton, Lewes Road, Brighton BN2 4GJ

Email: k.staines@brighton.ac.uk Tel: 01273 642 094

Hasmik Jasmine Samvelyan, University of Brighton, Lewes Road, Brighton BN2 4GJ

Email: h.samvelyan@brighton.ac.uk Tel: 01273 641 671

Funding

We are grateful to Medical Research Council (to KAS; MR/R022240/1), Tenovus Scotland, the Swedish Research Council (to AET; 2013–455) for funding.

Conflict of interest

The research leading to these results has received technical support from 3Dmagination Ltd, Didcot, UK. KM is co-founder and director of 3Dmagination Ltd in Oxford, UK, a company which provides training and consultancy in 3D and 4D imaging. The funding sources did not influence on the study design, data collection, analyses, interpretation, writing or submission of the manuscript.

Abstract

Objective: To investigate growth plate (GP) dynamics in surgical and loading murine models of osteoarthritis (OA), to understand whether abnormalities in these dynamics predict those at risk of OA.

Methods: 8-week-old C57BL/6 male mice underwent destabilization of medial meniscus (DMM) (n=8) surgery in right knee joints. Contralateral left knee joints had no intervention (controls). In 16-week-old C57BL/6 male mice (n=4), OA was induced using non-invasive mechanical loading of right knee joints with peak force of 11N. Non-loaded left knee joints were internal controls. Chondrocyte transiency in tibial articular cartilage (AC) and GP was examined by histology and immunohistochemistry. Tibial subchondral bone (SCB) parameters were measured using microCT and correlated to GP bridging.

Results: Higher expression of chondrocyte hypertrophy markers; Col10a1 and MMP13 were observed in tibial AC chondrocytes of DMM and loaded mice. In tibial GP, Col10a1 and MMP13 expressions were widely dispersed in a significantly enlarged zone of proliferative and hypertrophic chondrocytes (P>0.001). 3-dimensional quantification revealed enriched GP bridging and higher bridge densities in medial compared to lateral tibiae of DMM and loaded knee joints of the mice. GP dynamics were associated with increased SCB and epiphyseal trabecular bone volume fraction (BV/TV; %) in medial tibiae of DMM and loaded knee joints respectively.

Conclusions: Results confirm associations between aberrant chondrocyte hypertrophy marker expression and OA pathology in a surgical and loaded murine model of OA. Spatial variations in GP bridging formation revealed accelerated cartilage-bone transitions which may contribute to anatomical variation in vulnerability to OA development in these models.

Introduction

Osteoarthritis (OA) is a chronic musculoskeletal disease and a leading cause of disability and major healthcare costs in the world. It is estimated that worldwide 10% of men and 18% of women aged over 60 years have symptomatic OA (1) and, therefore, the predicted increase in the ageing population and longevity will result in a greater occurrence of the disease. OA is a complex disease in which the pathogenesis, cellular and molecular mechanisms of initiation and progression are not completely understood. It is characterised by progressive loss of articular cartilage (AC), formation of osteophytes, subchondral bone (SCB) sclerosis, synovial proliferation and inflammation and lax tendons. These can ultimately lead to a loss of joint function, pain, reduced mobility and disability (2). Despite the significant healthcare and economic burden there are few non-invasive therapies available to patients. Therefore, understanding the pathogenesis of OA and defining the molecular mechanisms underpinning AC degeneration can lead to the development of successful targeted and effective disease-modifying treatments.

Primary OA is described as naturally occurring OA affecting one joint (localised) or three or more joints (generalised), while secondary OA is associated with various causes and risk factors leading to the disease including trauma, obesity, diabetes, metabolic bone and congenital disorders (3). AC degeneration is one of the main hallmarks of OA and previous research has largely sought to identify mechanisms underpinning its deterioration. Fully developed, uncalcified AC is populated by a single resident cell chondrocytes, which maintain a stable phenotype characterised by small cell size and expression of tenascin-C (4). The inherent stability of AC chondrocytes ensures that dynamic events are restricted to assure lifelong articular integrity and healthy joint function. In contrast, epiphyseal growth plate (GP) chondrocytes have a transient phenotype to ensure long bone development (endochondral ossification) and growth. GP chondrocytes undergo a differentiation sequence

of proliferation, maturation and hypertrophy. The final stage of chondrocyte hypertrophy enables mineralisation of the cartilage extracellular matrix, vascular invasion and subsequent replacement of the mineralised cartilage anlagen with bone (5). These processes are coupled, however, with sexual maturation the human GP undergoes progressive narrowing as bony bridges form and span its width. This ultimately leads to complete GP closure and cessation of human growth. Indeed, in humans the longitudinal bone growth stops with the onset of puberty, the metaphysis then fuses with the epiphysis and the growth plate disappears (6). In mice, longitudinal bone growth does not cease at sexual maturity instead it slows dramatically at puberty, but the growth plates do not completely fuse and disappear (7).

We have previously shown that in the STR/Ort mouse, a naturally occurring OA murine model, AC chondrocytes transform from their inherently stable phenotype to a transient one, characteristic of the chondrocytes in the GP. This was confirmed by immunolabelling for chondrocyte hypertrophy markers; type X collagen (Col10a1) and matrix metalloproteinase 13 (MMP13) (8). Further, we revealed accelerated longitudinal bone growth, aberrant expression of growth plate markers (Col10a1 and MMP13) and increased growth plate chondrocyte maturation in these mice. Consistent with this, using a novel synchrotron computed tomography method we revealed enriched GP bone bridging in STR/Ort mouse tibiae indicative of advanced GP closure which may underpin OA (8,9).

Despite this, interlinks between the differing chondrocyte phenotypes in the AC and the GP, and the contribution that the GP may play in underpinning OA vulnerability is not yet understood. Indeed, understanding this will inform strategies for maintaining musculoskeletal health in ageing by potentially identifying whether GP dynamics may predict who is at risk of OA in later life and ultimately developing targeted OA treatments. Therefore, we hypothesised that surgically (destabilisation the medial meniscus [DMM]) or non-surgically

(mechanical loading) induced OA onset in C57BL/6 mice is linked to altered growth plate dynamics.

Materials and Methods

Animals

Male C57BL/6 wild type mice at 7 weeks of age (young adult) were obtained from Charles River Laboratories Inc. (Margate, UK). The mice were acclimatised to their surroundings for seven days. All mice were allowed free access to water and maintenance diet ad libitum (Special Diet Services, Witham, UK) in a 12-hour light/dark cycle at a room temperature of 21 ± 2^0C and relative humidity of 55 ± 10%. All procedures complied with the United Kingdom Animals (Scientific Procedures) Act 1986 and were approved by The University of Edinburgh Roslin Institute's Animal Users and Research Ethics Committees. All analyses were conducted blindly to minimise the effects of subjective bias.

The destabilisation of the medial meniscus (DMM)

A group of eight 8-week old wild type C57/BL6 male mice underwent DMM surgeries to induce OA-like changes in the right knee joints under isoflurane-induced anaesthesia. We chose not to performed SHAM (placebo) surgery on the left contralateral knee of the animals based upon animal welfare grounds since it was previously shown that there is no difference in OA scores between SHAM-operated and non-operated knee joints (10,11). Animals were randomly allocated to experimental groups to reduce subjective bias. Following transection of the medial meniscotibial ligament (MMTL) to destabilise the medial meniscus, the skin was closed and anaesthesia reversed (10). Eight weeks later, mice were sacrificed by exsanguination and confirmation of death by cervical dislocation. The knee joints of all the mice were dissected, fixed in 4% paraformaldehyde for 24 hours at 4^oC, and then stored in 70% ethanol.

In vivo loading of the knee joint

The right knee joints of 16-week-old wild type C57BL/6 male mice (n = 4) were subjected to non-invasive, dynamic axial mechanical loading under the isofluorane-induced anaesthesia (liquid isofluorane was vaporised to a concentration of 4% and maintained at a concentration of 2% with oxygen) for 7 min/day, 3 alternate days a week for 2 weeks according to the protocols described in the previous studies (12,13). The left knee joints were non-loaded internal controls in these animals. Briefly, using a servo-electric materials testing machine (Electroforce 3100, Bose, UK), axial compressive loads were applied through the right knee joint via customised concave cups which held the knee and ankle joints flexed and the tibiae vertically.

The tibia was held in place by continuous static preload of 0.5N onto which dynamic loads were superimposed in a series of 40 trapezoidal shaped waveform cycles with steep up and down ramps and a peak force of 11N for 0.05 seconds (0.025 seconds rise and fall time; 9.9 seconds baseline hold time between periods of peak loading). The right and left knees were dissected 3 days after the final loading episode. Mice were sacrificed by exsanguination and confirmation of death by cervical dislocation. Knee joints were fixed in 4% paraformaldehyde for 24 hours at 4^{o}C before being stored in 70% ethanol.

Micro-computed (microCT) tomography and 3-dimensional (3D) bridging analysis

Scans were performed with an 1172 X-Ray microtomograph (Bruker MicroCT, Kontich, Belgium) to evaluate the SCB and GP bridging. High-resolution scans with an isotropic voxel size of 5 µm were acquired (50 kV, 200 µA, 0.5 mm aluminium filter, 0.6° rotation angle). The projection images were reconstructed and binarised with a threshold of 0 to 0.16, ring artefact reduction was set at 10 and beam hardening correction at 0% using the SkyScan NRecon software package (v1.6.9.4, Bruker MicroCT). The images then were realigned vertically using DataViewer software (v1.5.1.2 64-bit, Bruker MicroCT) to ensure similar

orientation for analysis. Hand-drawn regions of interests (ROI) of the SCB and epiphyseal trabecular bone for each tibial lateral and medial compartments were selected (14). The structural parameters of tibial SCB plate and epiphyseal trabecular bone were calculated using 3D algorithms of SkyScan CTAn software (Bruker MicroCT) including SCB (SCB BV/TV; %) and trabecular bone volume fraction (Tb. BV/TV; %) and correlated to GP bridging analysis using a 3D synchrotron-computed tomography quantification method as previously described (15). Briefly, microCT scans of the tibiae were segmented using a region-growing algorithm within the Avizo® (V8.0, VSG, Burlington, VT, USA) software. The central points of each bony bridges were identified and projected on the tibial joint surface. The distribution of the areal number density of bridges (N, the number of bridges per 256 µm × 256 µm window; $d = m/V$) is then calculated and superimposed on the tibial joint surface (each bridge has a colour that represents the areal number density at the bridge location). The SCB plate and epiphyseal trabecular bone thickness (Th; mm) was determined and colour-coded thickness images were generated using the Avizo® software (15).

Histological analysis

The left and right knee joints of all the mice were decalcified in 10% ethylenediaminetetraacetic acid (EDTA) solution, wax-embedded at Leica EG1160 Tissue Embedding Station and 6 µm coronal sections cut using Leica RM2135 manual microtome.

Immunohistochemistry

Immunohistochemical analysis of chondrocyte transiency markers in tibial AC and GP was performed on 6 µm coronal sections using anti-matrix metalloproteinase 13 (anti–MMP13) (1:200 dilution; Abcam) or anti-collagen type X (anti-Col10a1) (1:100 dilution; Abcam) antibodies. As a control, an equal concentration of rabbit IgG was used. For immunohistochemical localisation of MMP13 and Col10a1, sections were dewaxed in xylene and rehydrated. Sections were incubated at 37 °C for 30 min in 1mg/ml trypsin for antigen

demasking. Endogenous peroxidases were blocked by treatment with 0.3% H_2O_2 in methanol (Sigma) for 30 min at room temperature. The Vectastain ABC universal detection kit (Vector Laboratories, Peterborough, UK) was used to detect the biotinylated secondary antibody (Anti-Mouse IgG Reagent) after incubation for 30 min at room temperature according to the manufacturer's instructions. Diaminobenzidine (DAB) solution used to detect the location of antigens. The sections were finally dehydrated, counterstained with haematoxylin and mounted in DePeX. All sections to be compared were immunolabelled at the same time to standardise conditions and minimise any differences in antibody incubation times.

GP zone analysis

The stained sections from the joints of 4 individual mice from each experimental group were used to measure the width of the GP proliferating and hypertrophic zones, as well as the total GP width, measured at 10 different points along the length of the GP in tibiae, using a light microscope and ImageJ software.

Statistical analysis

All analyses were performed with GraphPad Prism software 6.0f version (GraphPad Inc, La Jolla, CA, USA) using a two-sided 0.05 level of significance. The results were presented as the mean ± standard error of the mean (SEM). The Normal distribution of data was assessed using the Shapiro-Wilk normality test. For comparing two groups (experimental with control, or medial with the lateral compartment of tibiae), two-tail Student's *t*-test (paired or unpaired) was used. For comparing more than two groups, two-way ANOVA (analysis of variance) was used with Tukey post-hoc test.

Results

Transient chondrocyte behaviour in the tibial AC of DMM and loaded C57BL/6 young adult male mice

We first sought to confirm whether loss of AC in C57BL/6 mice with surgically and loading induced OA was associated with the expression of markers of transient chondrocyte phenotype. Immunohistochemistry analysis showed higher expression levels of well-established chondrocyte hypertrophy markers; Col10a1 and MMP13, observed in tibial AC of C57BL/6 mice that have undergone DMM surgery or mechanical loading compared with non-operated and non-loaded control left tibiae, respectively (Figure 1A, 1B). The expression pattern of Col10a1 was largely restricted to hypertrophic chondrocytes in the uncalcified zone of the AC of unaffected condyles of non-operated (Figure 1A) and non-loaded (Figure 1B) mouse left joints as expected (16). Whereas, the immunolabeling of Col10a1 was more widespread throughout the extracellular matrix (ECM) of the AC in affected right joints of DMM (Figure 1A) and loaded (Figure 1B) mice. Similarly, immunohistochemistry analysis showed positive MMP13 labelling in both superficial and deep articular chondrocytes in the right joints of DMM and loaded C57BL/6 male mice compared to the control knee joints (Figure 1A and B). These findings confirm an aberrant deployment of transient chondrocytes in uncalcified AC.

Dysfunctional GP morphology in DMM and loaded tibiae of C57BL/6 young adult male mice

In the tibial GP of mice with surgically and loading induced OA, Col10a1 expression was more greatly and widely dispersed throughout the zones of proliferative and hypertrophic chondrocytes compared with their controls (Figure 2A and 2B). Indeed, immunolabeling for Col10a1 revealed the expected localisation in the GP of non-operated and non-loaded mouse tibiae, limited primarily to the hypertrophic zone and underlying adjacent metaphyseal bone (Figure 2A and 2B). This disrupted the distribution of a GP zone marker was also evident for MMP13 in the GP of DMM and loaded C57BL/6 mouse tibiae compared to their controls (Figure 2A and 2B).

GP zone analysis revealed significantly enlarged proliferative and hypertrophic zones of chondrocytes in both DMM ($p<0.001$ and $p<0.0001$, respectively) and loaded (both $p<0.0001$) tibiae of C57BL/6 mice compared to their controls, and significantly increased total GP width (both $p<0.0001$) (Figure 3). Together, the results may indicate associations between dysfunctional GP morphology and marker expression, and OA development.

Associations between GP bridging in DMM and loaded tibiae of C57BL/6 young adult male mice and OA development

To further correlate aberrant longitudinal GP dynamics, GP bridging and OA development in these C57BL/6 young adult male mice, we used our newly developed 3D method to quantify bony bridges across the tibial epiphysis of DMM and loaded mice (Figure 4). 3D quantification revealed a significantly higher number of GP bridges in medial compared to lateral tibiae that underwent DMM surgeries (306 ± 32 versus 196 ± 33; $p<0.05$) (Figure 4B and 4E). This significant difference was not observed in non-operated tibiae (326 ± 32 versus 254 ± 32; $p>0.05$) (Figure 4A and 4E). Similarly, significantly enriched GP bridging was evident in the medial compartment of loaded tibiae in comparison to the lateral compartment (731 ± 19 versus 532 ± 56; $p<0.01$) (Figure 4D and 4E), and in those of non-loaded tibiae, although less pronounced than in the loaded right knee joints (782 ± 38 versus 614 ± 27; $p<0.05$) (Figure 4C and 4E). However, no significant differences in GP bridge numbers and densities were observed between interventions (DMM versus non-operated, and loaded versus non-loaded) at this time point in either the medial or lateral compartment. Anatomical variations were observed however with clusters forming in the medial anterior of loaded tibiae versus those more in the central and posterior of non-loaded tibiae (Figure 4C and 4D). Similarly, in the DMM tibiae, GP bridges were more widespread across the tibiae than in non-operated which were predominantly observed around the periphery (Figure 4A and 4B).

These results were consistent with the areal bridge density analysis. The mean areal bridge densities were significantly greater in medial compared to the lateral compartment of DMM (8.2 ± 0.9 versus 10.3 ± 0.9; $p<0.01$) and loaded tibiae (16 ± 0.9 versus 20.3 ± 0.6; $p<0.001$) (Figure 4F). However, no significant differences in the mean areal bridge densities were observed between interventions (DMM versus non-operated, and loaded versus non-loaded).

MicroCT analysis and 3D visualisation of SCB plate and epiphyseal trabecular bone

To establish whether aberrant GP dynamics are associated with the SCB plate and epiphyseal trabecular bone abnormalities after the DMM surgery and mechanical loading in our mice, we performed microCT analysis and determined local thickness of SCB plate and epiphyseal trabecular bone. The SCB plate volume fraction (SCB BV/TV) was significantly higher in medial compared to lateral compartment of DMM and non-operated tibiae (DMM: SCB BV/TV DMM: 29.42 ± 3.1% versus 36.72 ± 4.5%, $p<0.05$, non-operated: 35.67 ± 0.7% versus 42.57 ± 1.54%, $p<0.01$) (Figure 5A). No significant differences were observed between DMM and non-operated tibia (Figure 5A), or in the epiphyseal trabecular bone volume fraction (Tb. BV/TV; Figure 5B). Conversely, in the loaded and non-loaded tibiae, epiphyseal trabecular bone volume fraction (Tb. BV/TV) was significantly increased in the medial compared to lateral compartment (loaded: Tb. BV/TV 63.13 ± 1.2% versus 76.61 ± 2.7%, $p<0.01$, non-loaded: Tb. BV/TV 64.58 ± 1.4% versus 79.1 ± 3.2%, $p<0.01$) (Figure 5D). No significant differences were observed between interventions, or in the SCB BV/TV (Figure 5C). Colour-coded SCB plate thickness analysis revealed anatomical variation in SCB plate thickness between DMM and non-operated, and loaded and non-loaded plates (Figure 6A and 6B). Differences in the non-loaded and loaded SCB plates were particularly apparent (Figure 6B), and correlated with the clusters of higher density GP bridges previously observed (Figure 4C and 4D). Epiphyseal trabecular bone thickness was not significantly

altered in response to either invasive or non-invasive intervention (data not shown; Figure 6C and 6D).

Discussion

This study reveals altered GP dynamics in both surgical (DMM) and non-invasive loading murine *in vivo* models of OA, which with findings described above may indicate an endochondral defect in AC and GP cartilage in these mouse models of OA. Our data show changes in AC of the knee joints of these mice consistent with the aberrant deployment of hypertrophic chondrocytes. This is associated with disrupted GP morphology, increased GP chondrocyte differentiation indicated by widespread expression of chondrocyte hypertrophy markers and increased GP zone widths. Moreover, we have discovered enriched GP bony bridging indicative of premature GP fusion and accelerated growth cessation in the medial compartment of tibiae of these mice. These bridging events are spatially correlated with increases in SCB thickness. These data reveal that altered GP dynamics and spatial differences in GP bridging may contribute to an anatomical variation in vulnerability to OA development in surgical and loaded murine models of OA.

The STR/ort OA murine model is predisposed to developing spontaneous idiopathic OA whilst its nearest available parental strain, the CBA mouse, has a very low susceptibility which makes them effective controls for the studies (17). We have previously shown that aberrant deployment of transient chondrocyte behaviour, consistent with re-initiation of endochondral processes, occurs in uncalcified AC of STR/ort mouse knee joints compared to CBA controls (8). Here we extend these studies to look at the expression of transient markers in other stratifications of OA. Surgically induced DMM model is widely used for target validation studies or evaluation of the pathophysiological roles of many molecules in OA. Following DMM, medial displacement of the medial meniscus in a mouse knee joint provides

a smaller area to transmit the weight-bearing forces and leads to an increased local mechanical stress (18). Whereas, in a cyclic AC tibial compression model, the non-invasive dynamic mechanical loading applied to the mouse tibia through the knee and ankle joints, modifies AC structure locally through a mechanoadaptive homeostatic response contributing to OA development (19). Our findings in both surgical and non-invasive loading C57BL/6 mouse models are consistent with the evidence of the role of chondrocyte phenotype alterations in OA pathology. Hypertrophic chondrocytes in the calcified cartilage and GP of the healthy joints express Col10a1 (17–19). The calcified cartilage acts to protect the uncalcified AC through maintaining its ECM in an unmineralised state and the stability of the AC. However, hypertrophic differentiation of these chondrocytes contributes to AC matrix degradation, calcification and vascular invasion resulting in the demise of the AC (23). Consistent with this, the expression of Col10a1, as examined using immunohistochemistry, has been observed throughout AC in the joints of our both DMM and loaded mice. Further, the higher expression level of another marker of chondrocyte hypertrophy; MMP13 has been detected in superficial and uncalcified chondrocytes in the AC of DMM and loaded mice compared to their non-operated and non-loaded left knee joints. Indeed, cartilage degradation observed in OA has been attributed to an elevated production of proteolytic enzymes among which MMP13 has a major role (24,25). Studies using transgenic mice deficient in catabolic transcription factors that induce hypertrophic differentiation revealed that animals were protected against surgically and chemically induced OA further highlighting the role of transient chondrocytes in AC degradation (26,27).

The results of the present study indicate aberrant widespread expression of Col10a1 and MMP13 in the GP of DMM and loaded tibiae of C56BL/6 mice, compared to the GP of non-operated and non-loaded control knees. Indeed, the histomorphometric analysis also revealed that these mice display a significantly enlarged zone of proliferative and hypertrophic

chondrocytes, compared with the chondrocytes in the GP of control tibiae of both models. Similarly, a significantly increased cumulative GP width was observed in these models. Longitudinal bone growth is determined by the modifying number of chondrocytes in the proliferative zone of GP, rate of their proliferation, the extent of chondrocyte hypertrophy and controlled synthesis and degradation of ECM throughout the GP (28). Altered growth rate and mechanical modulation of GP function appear to result from complex interactions of changes in the states of these chondrocytes, as does the rate of growth plate closure due to the formation of bone bridges forming and spanning the width of the GP.

Our report of increased GP chondrocyte dynamics in these DMM and loaded C57BL/6 mice is further strengthened by our data acquired using a 3D quantification method of bony bridging across the tibial epiphysis, which showed premature GP closure in the medial compartment of the tibiae in all mice examined, regardless of intervention. This was indicated by significantly enriched spatial localisation of GP bone bridging clustering and number in the medial compared to the lateral compartments of DMM mice compared to non-operated mice. This is consistent with our previous work in the STR/Ort mouse model of spontaneous OA in which we observed similar spatial variations. We postulate that the formation of these bridges may be accelerated by local factors like instigating altered mechanoadaptive response and that these spatial variations in GP bridging may disclose the anatomical vulnerability to OA. These findings are supported by the previous studies suggesting associations between local mechanical stress caused by medial displacement of the medial meniscus (29) or cyclic tibial AC compression (19) and GP function in C57BL/6 mice. They are further supported by our previous work in which we revealed, by finite element modelling, that GP bridges act to dissipate stresses upon loading to the overlying SCB and thus suggest that this contributes to OA seen in these models. These studies have, for the first time, shown that accelerated GP closure is indicative of modified growth

dynamics in the right tibiae of both surgical and loading murine models of OA. This is consistent with our microCT analysis of spatial variations in SCB plate thickening in these animals, and its correlation to GP bridges. We observed statistically significant changes in subchondral bone parameters in medial compared to lateral compartment including subchondral bone volume fraction in the tibiae of DMM mice and epiphyseal trabecular bone volume fraction in the tibiae of loaded mice. It was previously shown that SCB thickening may be intensified by adjacent AC lesions following mechanical trauma thus indicating a special link between changes in SCB architecture and AC lesions in OA pathology (14).

However, the limitation of this study is that we only examined the GP at one specific time point for each model and therefore more time points are required to understand how these GP bridges temporally affect SCB changes and OA pathology. With its controllability, the intermittent non-invasive mechanical loading model will allow in future to distinguish between short- and long-term effects of various cyclic loading regimens on subchondral and trabecular bone parameters as well as AC integrity, GP dynamics and correlate these to initiation and progression of human OA. Indeed, it is known that in the loading model, the short-term intervention is not sufficient to induce changes in subchondral thickness and thus longer intervention times for both the DMM and loading models may also prove useful in pursuit of understanding these relationships (14).

Taken together, our studies indicate that accelerated GP chondrocyte dynamics and bridging events may contribute to OA pathology in both surgical and loading C57BL/6 mouse OA models and that similar osteoarthritic pathological changes happen in different *in vivo* models of secondary (post-traumatic) OA (18) through inducing direct (DMM) or indirect (mechanical loading) injuries to the joints. The GP bony bridging analysis may signify accelerated cartilage-bone transition and growth cessation in these affected bones advancing our understanding of GP closure mechanisms and how these contribute to the health of the

joint. Further, our work yields more insights into the changes in the micro-mechanical environment of the GP and cells, specifically chondrocytes, within the GP.

Nonetheless, whether modified GP trajectories are prevalent in human OA is yet to be defined and studies determining associations between GP dynamics during adolescence and OA development in human patients would allow elucidation of the pathogenesis of OA and will ultimately enable the development of novel and specific therapeutic interventions.

Acknowledgements

The authors would like to thank The Roslin Institute of The University of Edinburgh for the assistance with the care of animal models in this study.

Author contributions

All authors contributed to the study design, analysis and interpretation of the data, drafted, critically reviewed, edited and approved the version of the manuscript for publication.

References

1. Murray CJ., Lopez AD. Global Burden of Disease and Injur Y Series the Global Burden of Disease. *Oms* 1996:1–46.

2. Goldring MB, Goldring SR. Osteoarthritis. *J Cell Physiol* 2007;213:626–634.

3. Altman R, Asch E, Bloch D, Bole G, Borenstein D, Brandt K, et al. Development of criteria for the classification and reporting of osteoarthritis: Classification of osteoarthritis of the knee. *Arthritis Rheum* 1986;29:1039–1049.

4. Pacifici M, Koyama E, Shibukawa Y, Wu C, Tamamura Y, Enomoto-Iwamoto M, et al. Cellular and molecular mechanisms of synovial joint and articular cartilage formation. *Ann N Y Acad Sci* 2006;1068:74–86.

392 5. Staines KA, MacRae VE, Farquharson C. The importance of the SIBLING family of
393 proteins on skeletal mineralisation and bone remodelling. *J Endocrinol* 2012;214:241–255.

394 6. Parfitt AM. Misconceptions (1): Epiphyseal fusion causes cessation of growth. *Bone*
395 2002;30:337–339.

396 7. Glatt V, Canalis E, Stadmeyer L, Bouxsein ML. Age-related changes in trabecular
397 architecture differ in female and male C57BL/6J mice. *J Bone Miner Res* 2007;22:1197–
398 1207.

399 8. Staines KA, Madi K, Mirczuk SM, Parker S, Burleigh A, Poulet B, et al. Endochondral
400 Growth Defect and Deployment of Transient Chondrocyte Behaviors Underlie Osteoarthritis
401 Onset in a Natural Murine Model. *Arthritis Rheumatol* 2016;68:880–891.

402 9. Madi K, Staines KA, Bay BK, Javaheri B, Geng H, Bodey AJ, et al. In situ
403 characterization of nanoscale strains in loaded whole joints via synchrotron X-ray
404 tomography. *Nat Biomed Eng* 2019;4:343–354.

405 10. Glasson BVSc SS, Blanchet BS TJ, Morris DVM EA. The surgical destabilization of the
406 medial meniscus (DMM) model of osteoarthritis in the 129/SvEv mouse. *Osteoarthr Cart*
407 2007;15:1061–1069.

408 11. Staines KA, Ikpegbu E, Törnqvist AE, Dillon S, Javaheri B, Amin AK, et al. Conditional
409 deletion of E11/podoplanin in bone protects against load-induced osteoarthritis. *BMC*
410 *Musculoskelet Disord* 2019;20:1–11.

411 12. Sugiyama T, Price JS, Lanyon LE. Functional adaptation to mechanical loading in both
412 cortical and cancellous bone is controlled locally and is confined to the loaded bones. *Bone*
413 2010;46:314–321.

13. Poulet B, Hamilton RW, Shefelbine S, Pitsillides AA. Characterizing a novel and adjustable noninvasive murine joint loading model. *Arthritis Rheum* 2011;63:137–147.

14. Poulet B, Souza R de, Kent A V, Saxon L, Barker O, Wilson A, et al. Intermittent applied mechanical loading induces subchondral bone thickening that may be intensified locally by contiguous articular cartilage lesions. *Osteoarthr Cartil* 2015;23:940–8.

15. Staines KA, Madi K, Javaheri B, Lee PD, Pitsillides AA. A computed microtomography method for understanding epiphyseal growth plate fusion. *Front Mater* 2018;4.

16. Chambers MG, Kuffner T, Cowan SK, Cheah KSE, Mason RM. Expression of collagen and aggrecan genes in normal and osteoarthritic murine knee joints. *Osteoarthr Cartil* 2002;10:51–61.

17. Poulet B, Westerhof TAT, Hamilton RW, Shefelbine SJ, Pitsillides AA. Spontaneous osteoarthritis in Str/ort mice is unlikely due to greater vulnerability to mechanical trauma. *Osteoarthr Cartil* 2013;21:756–763.

18. Samvelyan HJ, Hughes D, Stevens C, Staines KA. Models of Osteoarthritis: Relevance and New Insights. *Calcif Tissue Int* 2020. Available at: https://doi.org/10.1007/s00223-020-00670-x.

19. Poulet B, Hamilton RW, Shefelbine S, Pitsillides AA. Characterizing a novel and adjustable noninvasive murine joint loading model. *Arthritis Rheum* 2011;63:137–147.

20. Atkins GJ, Rowe PS, Lim HP, Welldon KJ, Ormsby R, Wijenayaka AR, et al. Sclerostin is a locally acting regulator of late-osteoblast/preosteocyte differentiation and regulates mineralization through a MEPE-ASARM-dependent mechanism. *J Bone Miner Res* 2011;26:1425–1436.

436 21. Lai Y, Bai X, Zhao Y, Tian Q, Liu B, Lin EA, et al. ADAMTS-7 forms a positive
437 feedback loop with TNF-α in the pathogenesis of osteoarthritis. *Ann Rheum Dis*
438 2014;73:1575–1584.

439 22. Lu Y, Ding M, Li N, Wang Q, Li J, Li X, et al. Col10a1-runx2 transgenic mice with
440 delayed chondrocyte maturation are less susceptible to developing osteoarthritis. *Am J Transl*
441 *Res* 2014;6:736–745.

442 23. Ea HK, Nguyen C, Bazin D, Bianchi A, Guicheux J, Reboul P, et al. Articular cartilage
443 calcification in osteoarthritis: Insights into crystal-induced stress. *Arthritis Rheum*
444 2011;63:10–18.

445 24. Ortega N, Behonick DJ, Werb Z. Matrix remodeling during endochondral ossification.
446 *Trends Cell Biol* 2004;14:86–93.

447 25. Stickens D, Behonick DJ, Ortega N, Heyer B, Hartenstein B, Yu Y, et al. Altered
448 endochondral bone development in matrix metalloproteinase 13-deficient mice. *Development*
449 2004;131:5883–5895.

450 26. Saito T, Fukai A, Mabuchi A, Ikeda T, Yano F, Ohba S, et al. Transcriptional regulation
451 of endochondral ossification by HIF-2α during skeletal growth and osteoarthritis
452 development. *Nat Med* 2010;16:678–686.

453 27. Yang S, Kim J, Ryu JH, Oh H, Chun CH, Kim BJ, et al. Hypoxia-inducible factor-2α is a
454 catabolic regulator of osteoarthritic cartilage destruction. *Nat Med* 2010;16:687–693.

455 28. Breur GJ, Lapierre MD, Kazmierczak K, Stechuchak KM, McCabe GP. The domain of
456 hypertrophic chondrocytes in growth plates growing at different rates. *Calcif Tissue Int*
457 1997;61:418–425.

458 29. Huang H, Skelly JD, Ayers DC, Song J. Age-dependent Changes in the Articular
459 Cartilage and Subchondral Bone of C57BL/6 Mice after Surgical Destabilization of Medial
460 Meniscus. *Sci Rep* 2017;7:1–9. Available at: http://dx.doi.org/10.1038/srep42294.

461 **Figure legends**

462 **Figure 1A, 1B.** Immunohistochemical labelling for type X collagen (Col10a1) and matrix
463 metalloproteinase (MMP13) in the articular cartilage of non-operated and DMM (A), or non-
464 loaded and mechanically loaded (B) knee joints of C57BL/6 male mice. Arrows indicate
465 examples of positive staining in the tibiae. Images are representative of results in 3 individual
466 mice. Scale bar = 200μm

467 **Figure 2A, 2B.** Immunohistochemical labelling for type X collagen (Col10a1) and matrix
468 metalloproteinase (MMP13) in the growth plate of DMM and non-operated (A), or
469 mechanically loaded and non-loaded (B) knee joints of C57BL/6 male mice. Arrows indicate
470 examples of positive staining in the tibiae. Images are representative of results in 3 individual
471 mice. Scale bar = 200μm. PZ = proliferative zone; HZ = hypertrophic zone.

472 **Figure 3.** Growth plate zone width of non-operated and DMM, or non-loaded and loaded
473 knee joints of C57BL/6 male mice. Ten measurements per section were obtained along the
474 length of the growth plate of the tibiae (n=4 mice for each experimental group). PZ =
475 proliferative zone; HZ = hypertrophic zone **** $p<0.0001$

476 **Figure 4A, 4B, 4C, 4D, 4E, 4F.** Location and areal densities of bridges across the growth
477 plate projected on the medial (M) and lateral (L) tibial joint surface in non-operated (A),
478 DMM (B), non-loaded (C) and loaded (D) tibiae of mice at 16 and 18 weeks of age, number
479 of bridges in lateral and medial tibiae of non-operated compared to DMM and non-loaded
480 compared to loaded tibiae of mice (E), Areal density (d) of bridges in medial compared to

lateral tibiae, defined as the number of bridges per 256 mm x 256 mm window of non-operated and DMM or non-loaded and loaded knee joints (F). Bars represent mean ± SEM. Group sizes were $n = 8$ for non-operated and DMM-operated mice and $n = 4$ for non-loaded and loaded mice. * $p<0.05$ ** $p<0.01$ *** $p<0.001$

Figure 5A, 5B, 5C, 5D. MicroCT analysis of the epiphyseal region of the lateral and medial tibiae in non-operated controls and DMM-operated knee joints subchondral bone volume fraction (SCB BV/TV) (A) and epiphyseal trabecular bone volume fraction (Tb. BV/TV) (B). MicroCT analysis of the epiphyseal region of the medial and lateral tibiae in non-loaded controls and loaded knee joints subchondral bone volume fraction (SCB BV/TV) (C) and epiphyseal trabecular bone volume fraction (Tb. BV/TV) (D). Bars represent mean ± SEM. Group sizes were $n = 8$ for non-operated and DMM-operated mice and $n = 4$ for non-loaded and loaded mice. * $p<0.05$ ** $p<0.01$

Figure 6A, 6B, 6C, 6D. Representative colour coded images of lateral and medial subchondral bone plate thickness of non-operated and DMM-operated tibiae of mice (A). Representative colour coded images of lateral and medial subchondral bone plate thickness of non-loaded and loaded tibiae of mice (B). Representative colour coded images of epiphyseal trabecular bone thickness of non-operated and DMM-operated (C), or non-loaded and loaded tibiae of mice (D).

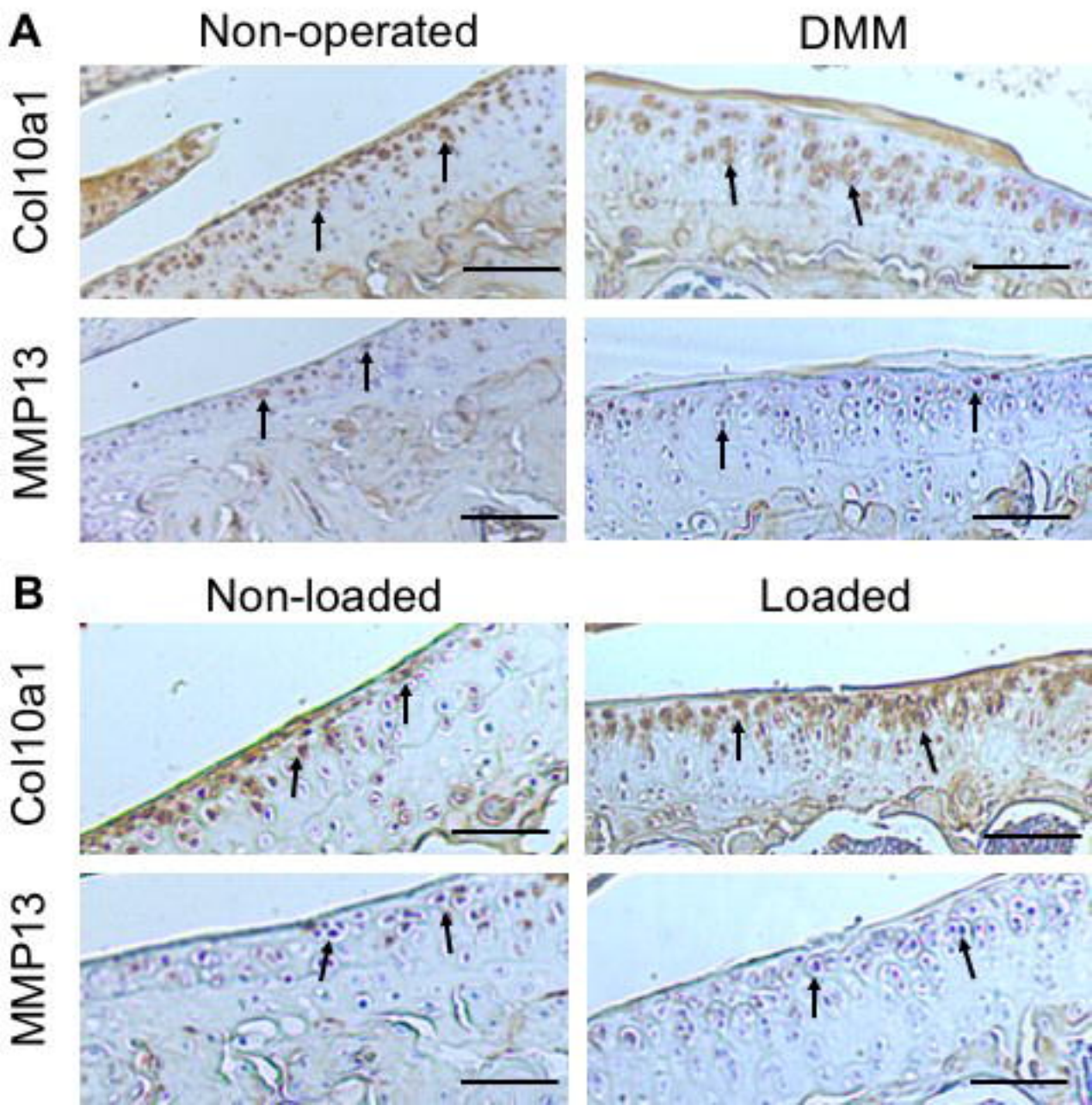
A
Non-operated
DMM
Col10a1
MMP13
B
Non-loaded
Loaded
Col10a1
MMP13

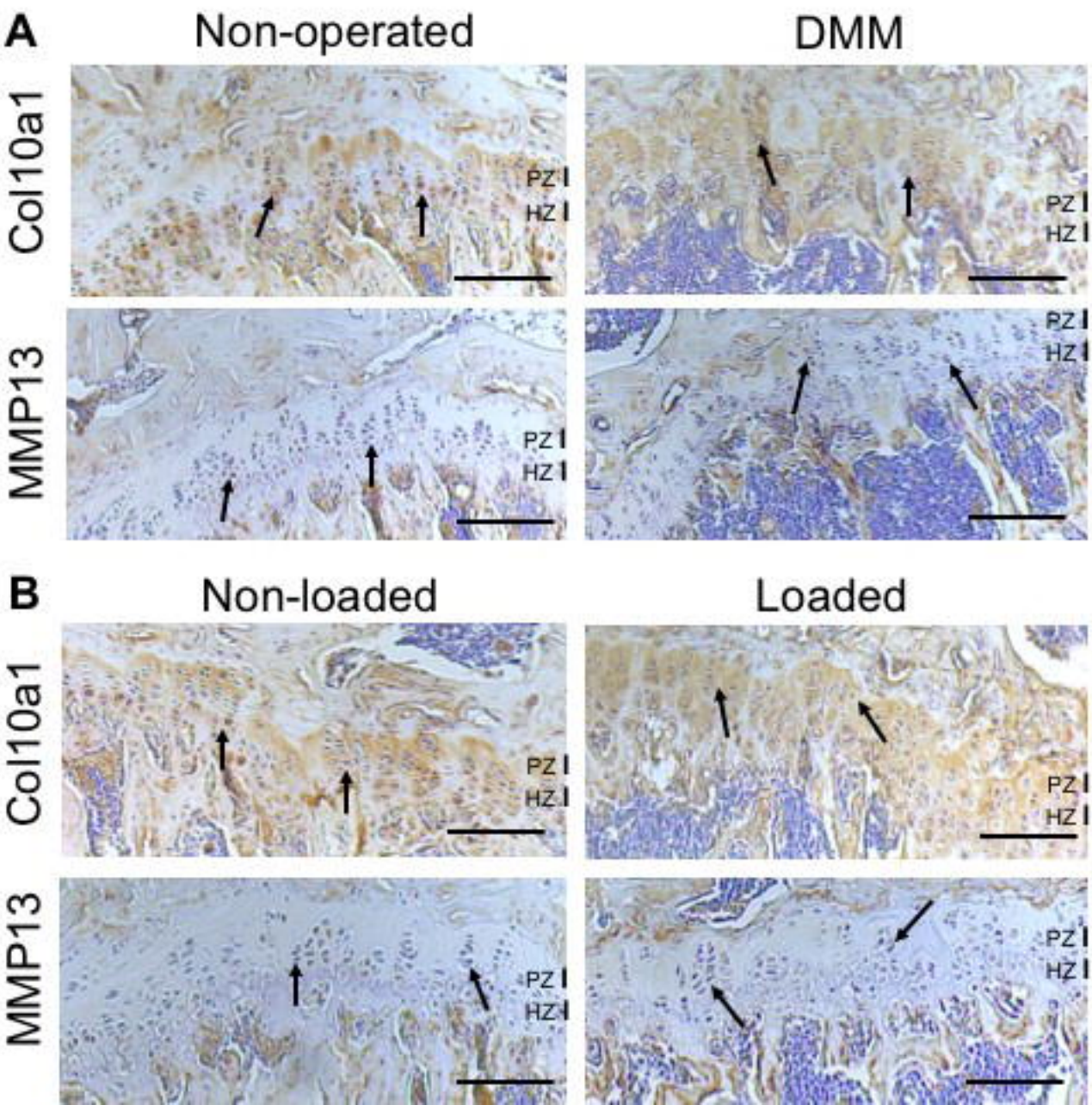
A
Non-operated
DMM
Col10a1
MMP13
PZ
HZ
B
Non-loaded
Loaded
Col10a1
MMP13
PZ
HZ

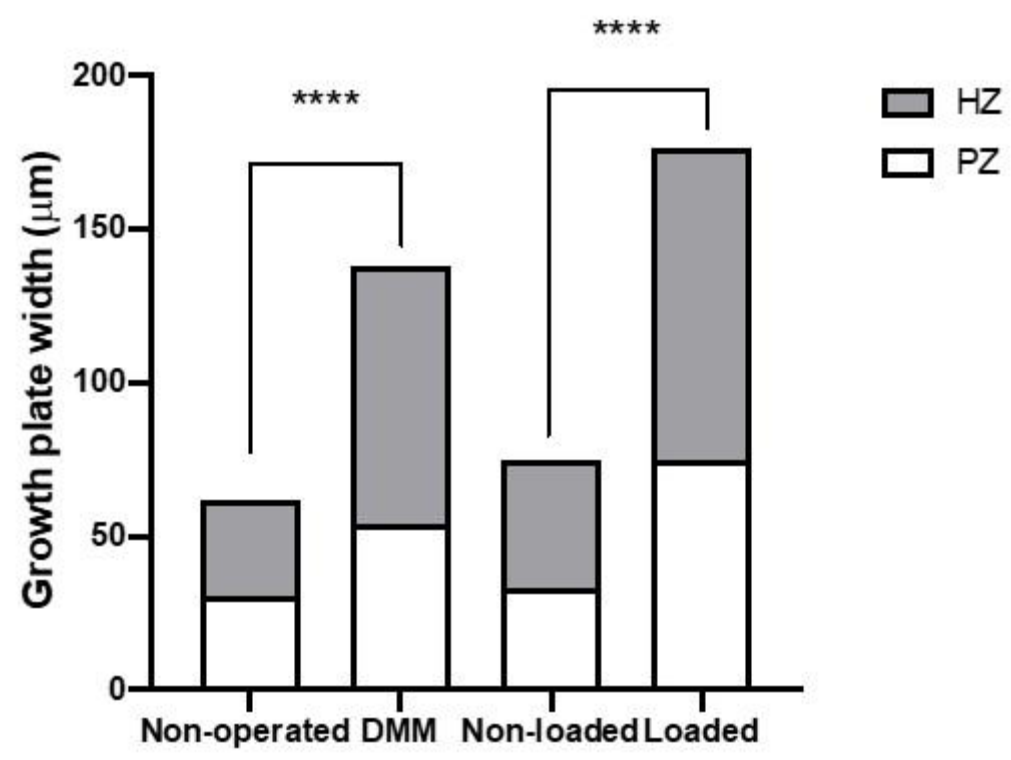
****
****
200
150
100
50
0
Growth plate width (μm)
HZ
PZ
Non-operated
DMM
Non-loaded
Loaded

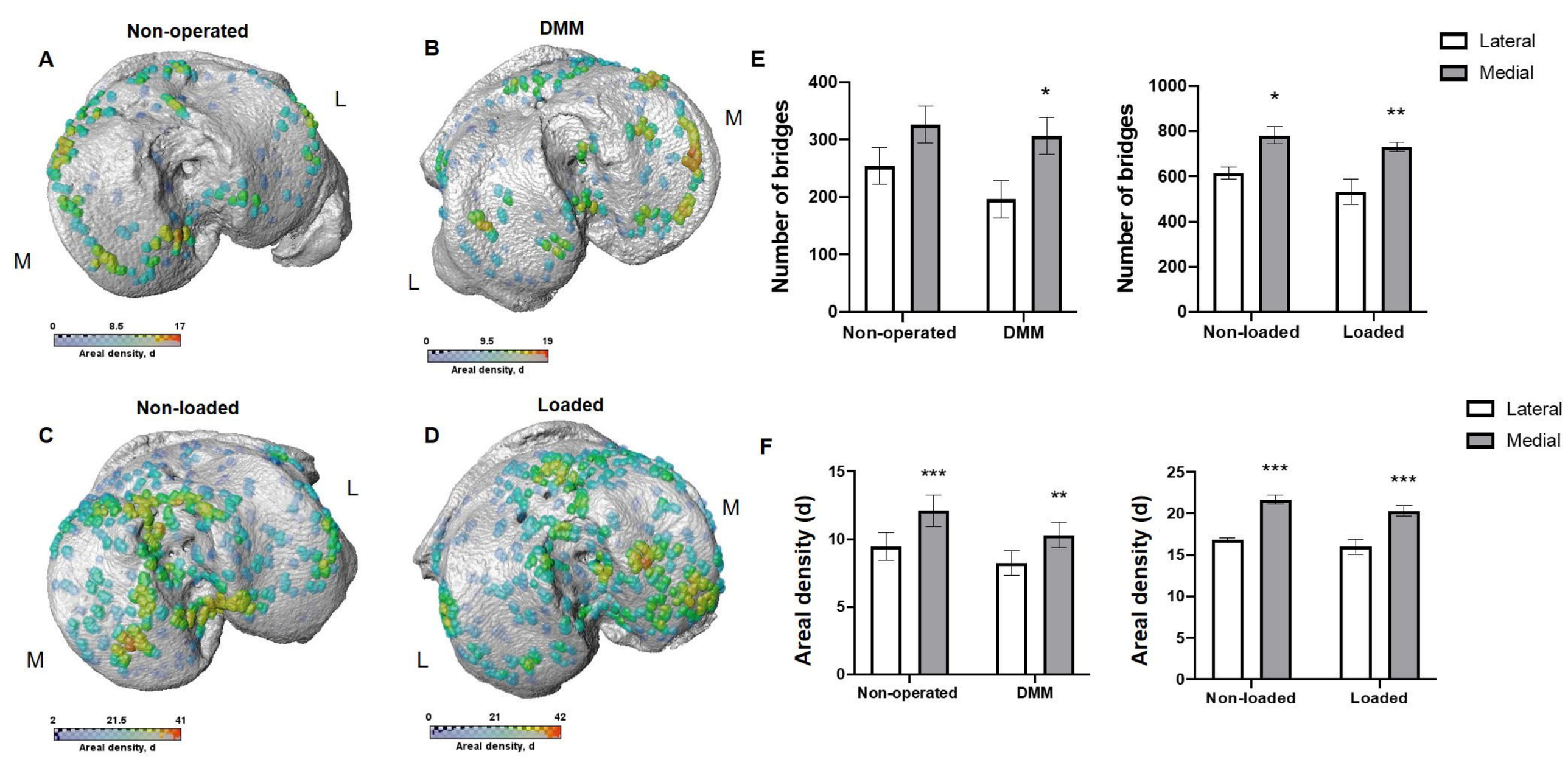
Non-operated
A
L
M
0
8.5
17
Areal density, d
DMM
B
M
L
0
9.5
19
Areal density, d
Non-loaded
C
L
M
2
21.5
41
Areal density, d
Loaded
D
M
L
0
21
42
Areal density, d
E
Lateral
Medial
Number of bridges
400
300
200
100
0
*
Non-operated
DMM
Number of bridges
1000
800
600
400
200
0
*
**
Non-loaded
Loaded
F
Lateral
Medial
Areal density (d)
15
10
5
0
***
**
Non-operated
DMM
Areal density (d)
25
20
15
10
5
0
***
***
Non-loaded
Loaded

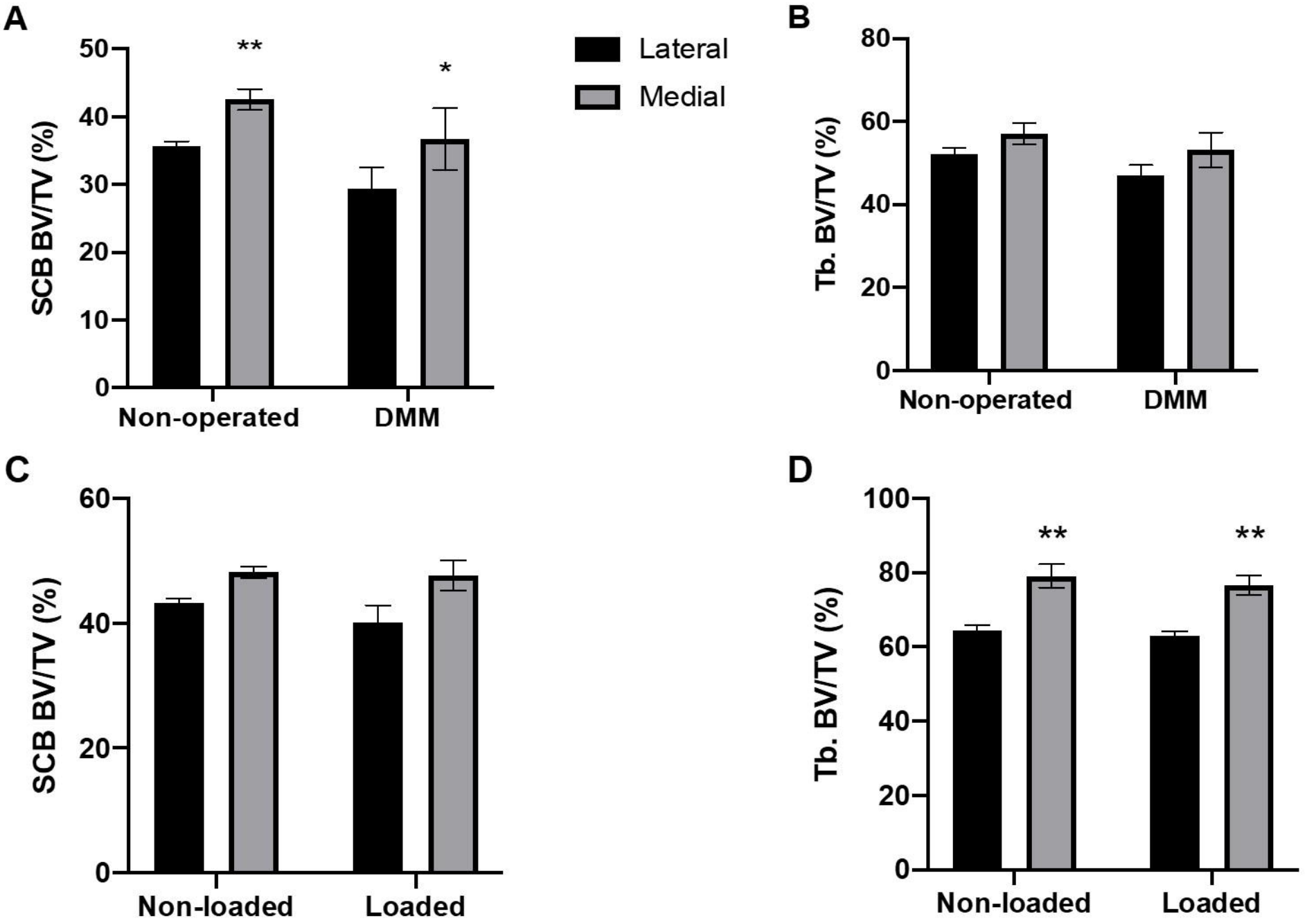
A
B
C
D
Lateral
Medial
SCB BV/TV (%)
Tb. BV/TV (%)
Non-operated
DMM
Non-loaded
Loaded
**
*
**
**
0
10
20
30
40
50
60
80
100

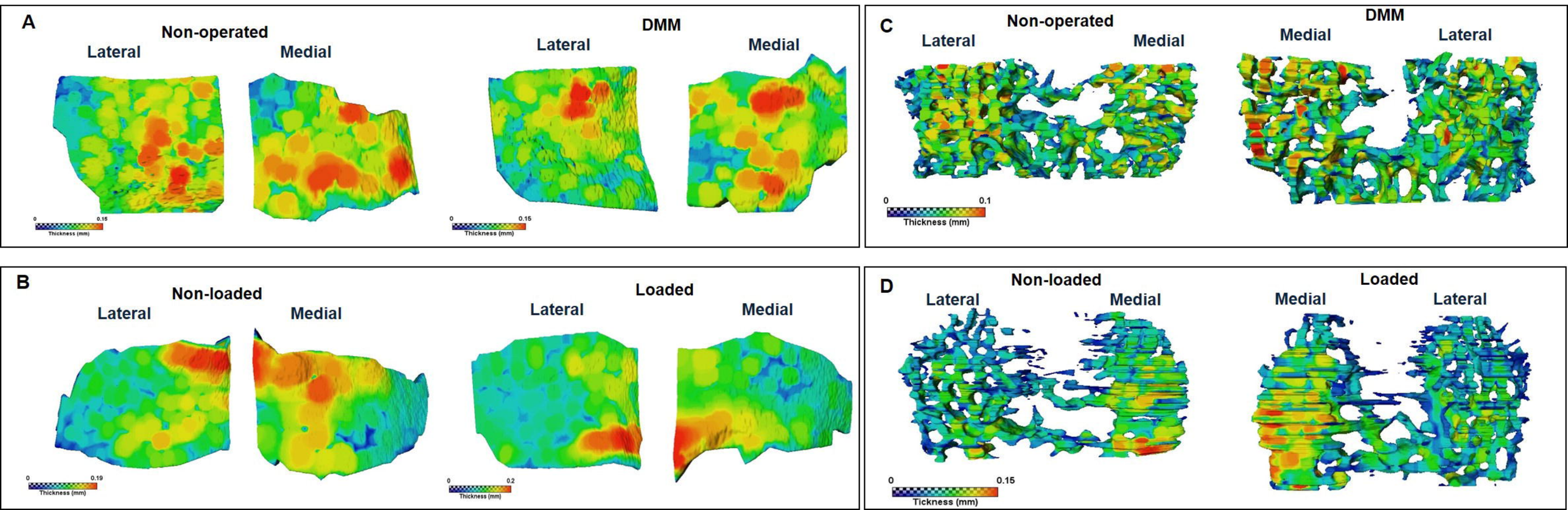
A
Non-operated
Lateral
Medial
0
0.15
Thickness (mm)
DMM
Lateral
Medial
0
0.15
Thickness (mm)
C
Non-operated
Lateral
Medial
0
0.1
Thickness (mm)
DMM
Medial
Lateral
B
Non-loaded
Lateral
Medial
0
0.19
Thickness (mm)
Loaded
Lateral
Medial
0
0.2
Thickness (mm)
D
Non-loaded
Lateral
Medial
0
0.15
Tickness (mm)
Loaded
Medial
Lateral